Journal of Intelligent Material Systems and Structures OnlineFirst, published on August 6, 2009 as doi:10.1177/1045389X09343022

Modeling and Characterization of a Linear Piezomotor

Mustafa Arafa,[1] Osama Aldraihem[2] and Amr Baz[3,*]

[1]*Mechanical Engineering Department, American University in Cairo, Egypt*

[2]*Mechanical Engineering Department, King Saud University, Kingdom of Saudi Arabia*

[3]*Mechanical Engineering Department, University of Maryland, USA*

ABSTRACT: This article presents the modeling and characterization of a new class of piezoelectric linear motor. The motor relies in its operation on a set of piezoelectric bimorphs which are sequentially activated to linearly move a drive rod along spring loaded rollers. Emphasis in this article is placed on studying the dynamic behavior of this class of piezoelectric motors, both theoretically and experimentally, in an effort to predict the piezomotor response to various loads and excitation schemes. To this end, a numerical model has been developed to simulate the dynamics of the piezoelectric bimorphs comprising the piezomotor. Friction between the bimorph elements and the drive rod are handled using an appropriate friction model. Experimental testing of the motor is carried out to validate the predictions of the theoretical model.

Key Words: piezoelectric motor, piezoelectric bimorphs, linear motion, dynamic modeling, finite element model, experimental validation.

NOMENCLATURE

$[C]$	Damping matrix
d_{33}	Piezoelectric strain constant
E	Young's modulus
E_3	Electric field
f	Friction force
F	Axial force
h	Bimorph height
I	Second moment of area of one bimorph layer
$[K]$	Stiffness matrix
L	Bimorph length
L_o	External load on drive rod
M	Bending moment
$[M]$	Mass matrix
N	Normal force by drive rod on bimorph
S_{33}^E	Compliance at constant electric field
S_3	Strain
T_3	Stress
$\{u(t)\}$	Load vector
v	Drive rod velocity
v_s	Slip velocity
V	Bimorph tip velocity
w	Bimorph out-of-plane width
x	Axial displacement
y	Transverse displacement
$\{\delta\}$	Vector of structural degrees of freedom
ε	Axial strain
μ	Coefficient of friction

INTRODUCTION

The quest for designing miniature mobility platforms has been a significant driving force for the development of reliable actuators and sensors to fit these modern applications. Among the promising designs are those relying on smart structures for their operation. One appealing embodiment of the vast literature on smart systems is the use of piezoelectric bimorphs since they offer various benefits over other designs such as the piezoelectric ultrasonic wave motors. For example, the bimorph motors provides high output power for a given torque and requires lower applied electric field (Tieck et al., 2007). Furthermore, the bimorph motors are generally very stiff and stable enabling very accurate load positioning with accuracies which are in the neighborhood of 10 nm (http://www.piezomotor.se/). However, these performance metrics occur at the expense of higher motor weight, low travel speeds, and low overall efficiency (Tieck et al., 2007).

The modeling of piezoelectric bimorphs has received considerable attention in the last two decades. An early model has been presented by Smits et al. (1991) where the effective shear forces and bending moments acting on a bimorph were obtained using force balance to

*Author to whom correspondence should be addressed.
E-mail: baz@umd.edu
Figures 1–11 appear in color online: http://jim.sagepub.com

1045-389X/09/00 0001–9 $10.00/0 DOI: 10.1177/1045389X09343022

predict the tip displacement under different static mechanical and electrical loads. Youn and Becker (1991) developed a finite element model to study the dynamics of piezoelectric bimorphs, accounting for the variation of electric field across the thickness of a piezoelectric beam. More recently, Wang (2004) presented a finite element formulation for the static and dynamic analysis of piezoelectric bimorph beams and plates. The use of such bimorphs in the form of legs for walking robots has been presented, for example, by Tani (1996). Another interesting design is attained by using the bimorphs in friction-driven high-precision actuators (Chang and Youcef-Toumi, 1998). The idea was further developed, improved, and applied by Bexell and Johansson (1999) to form a miniature rotary piezomotor and by Johansson et al. (2002) and Simu and Johansson (2006) who developed a friction-driven linear motor. Recent improvements of the idea are summarized in the U.S patent by Johansson et al. (2008)

It is important here to note that development of the piezoelectric bimorph motor has been limited to fabrication and evaluation (Simu and Johansson, 2002; Friend et al., 2004), quasi-static analysis of the motor dynamics (Simu and Johansson, 2006), or system identification and control (Merry et al., 2009).

In this study, however, the emphasis is placed on comprehensive theoretical and experimental investigation of the dynamic characteristics of this class of motors. In particular, a detailed coupled-field finite element model is developed to study the dynamics of piezoelectric bimorphs. Friction between the bimorph elements and the drive rod is also studied in an attempt to characterize the load–speed relationship of the linear motor. Comparisons are established between the theoretical predictions and the experimental results in order to validate the developed finite element model.

Such an effort is aimed to parallel the efforts exerted by Vinhais et al. (2004) to analyze the horn type piezomotor developed by Hill (2002) which has lower load capacity, lower output power, and higher applied electric field than the piezoelectric bimorph motor (Tieck et al., 2007).

This remainder of this article is organized into three sections. The dynamic model is introduced in section 'materials and methods'. The main results are presented in Section 'results and discussion', followed by discussions and conclusions.

DYNAMIC MODEL

Figure 1 shows a photograph and a schematic drawing of the piezoelectric motor under consideration. The motor consists of four piezoceramic bimorphs that are sequentially actuated to move a drive rod in a linear fashion. The piezomotor relies on friction forces between the drive rod and the piezoelectric bimorphs (legs) and contact is maintained by a set of two spring-loaded rollers, as shown in Figure 1.

By applying properly controlled and phase-shifted electric fields, the bimorphs can bend, elongate, and/or shrink. The combined motion of the bimorphs in pairs makes the bimorphs lift and push or lower and rest the drive rod. This two-by-two bimorph motion makes the motor run forwards or backwards, taking steps typically no bigger than 3–5 micrometers and reaching speeds of ~5–10 mm/s (http://www.piezomotor.se/).

Each bimorph in the present design consists of alternating active piezoelectric elements and electrodes, in the manner depicted in Figure 2, forming two multilayer piezoceramic stacks. Each stack has a length L, height h, and out-of-plane width w, and can be activated independently. It is assumed that the upper and lower stacks are made of the same piezoelectric material and have identical geometries. Bonding of all layers is assumed to be perfectly cohesive. Shear deformation and rotary inertia effects are included in the present model. A constant electric field across each individual piezoelectric layer is assumed since the variation across the small spacing between the electrodes forming the bimorph can be negligible, especially for low

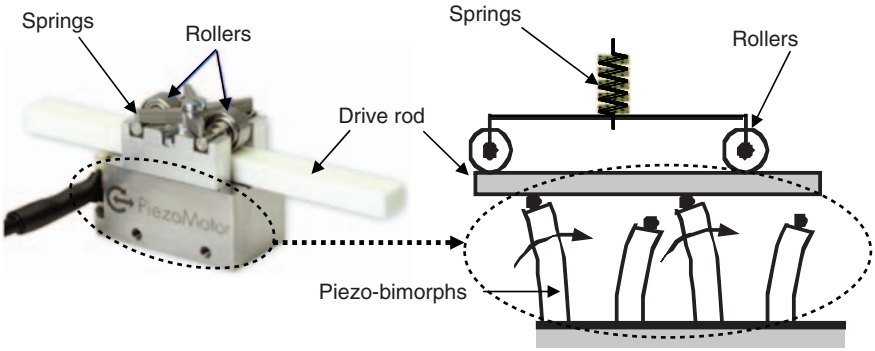

Figure 1. *Photograph of a linear piezoelectric motor (Johansson et al., 2004; PiezoLEGS, 2009).*

drive frequencies. The external loads imposed on the bimorphs during operation are those due to (a) applied electric field, (b) axial loading by the drive rod, and (c) transverse friction forces. The response of the bimorph to each of these effects is to be studied herein in order to predict the dynamic behavior of the piezomotor.

The pertinent piezoelectric constitutive equations for a d_{33} piezoceramic are given by,

$$\begin{aligned} \{T_3\} &= [c]\{S_3\} - [e]^T\{E_3\} \\ \{D\} &= [e]\{S_3\} + [\varepsilon]\{E_3\} \end{aligned} \tag{1}$$

where $\{T_3\}$,$\{S_3\}$denote the longitudinal stress and strain, $[c]$ is the compliance, $\{E_3\}$ is the effective electric field, $\{D\}$ is the electric displacement, $[e]$ is the piezo-electric coupling constant, and $[\varepsilon]$ is the permittivity.

A finite element coupled-field formulation is developed to model the dynamics of the piezoelectric bimorph. For the mechanical domain, the bimorph is modeled as an equivalent single layer using 1D Timoshenko beam elements having 3 degrees of freedom per node denoting the axial, transverse, and angular displacements. The displacements at any point within the element are interpolated by:

$$\begin{aligned} u &= \alpha_1 + \alpha_2 x, \\ v &= \beta_1 + \beta_2 x + \beta_3 x^2 + \beta_4 x^3 \\ \theta &= \gamma_1 + \gamma_2 x + \gamma_3 x^2 \end{aligned} \tag{2}$$

In this way, the structural displacements can be expressed in terms of the nodal degrees of freedom through the shape functions given by:

$$\begin{aligned} u &= \{N_{u1}\}\{\delta_u^e\} \\ v &= \{N_{u2}\}\{\delta_u^e\} \\ \theta &= \{N_{u3}\}\{\delta_u^e\} \end{aligned} \tag{3}$$

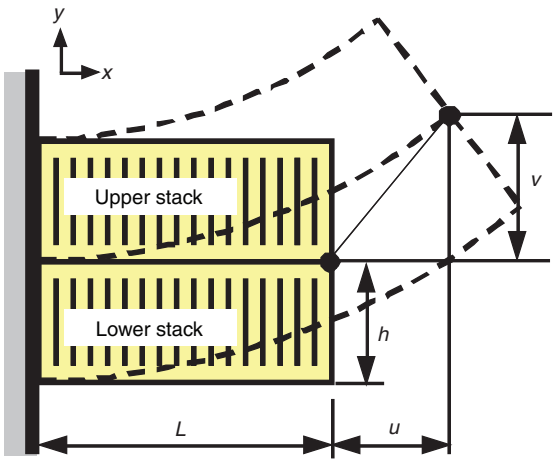

Figure 2. *Bimorph consisting of two piezoelectric stacks.*

where $\{\delta_u^e\}$ is the vector of nodal structural degrees of freedom. As the upper and lower stacks are activated independently, two additional electrical degrees of freedom are added at each node to designate the electric displacement of the upper and lower stacks. The electric displacements are assumed to be linearly interpolated along the element length through:

$$\begin{aligned} D^U &= \varphi_1 + \varphi_2 x \\ D^L &= \varphi_3 + \varphi_4 x \end{aligned} \tag{4}$$

where the superscripts U and L designate the upper and lower piezoelectric stacks, respectively. In this way, the electric displacement shape functions are given by:

$$\begin{aligned} D^U &= \{N_{d1}\}\{\delta_d^e\} \\ D^L &= \{N_{d2}\}\{\delta_d^e\} \end{aligned} \tag{5}$$

where $\{\delta_d^e\}$ denotes vector of nodal electrical degrees of freedom. Accordingly, the bimorph element developed herein possesses 5 degrees of freedom per node.

The mechanical strain energy due to axial, bending and shear effects in the bimorphs given by (Petyt, 1990):

$$\begin{aligned} U_{\text{mech}} = \frac{1}{2}\int_0^L \left[EA\left(\frac{\partial u}{\partial x}\right)^2 + EI\left(\frac{\partial \theta}{\partial x}\right)^2\right] \mathrm{d}x \\ + \frac{1}{2}\int_0^L \left[\kappa AG\left(\frac{\partial v}{\partial x} - \theta\right)^2\right] \mathrm{d}x \end{aligned} \tag{6}$$

Imposing the shape functions defined in Equation (3) gives:

$$U_{\text{mech}} = \frac{1}{2}\left\{\delta_u^e\right\}^T [K_{uu}^e]\left\{\delta_u^e\right\} \tag{7}$$

where:

$$\begin{aligned} \left[K_{uu}^e\right] = \frac{1}{2}\int_0^L [EA\{N_{u1_{,x}}\}^T\{N_{u1_{,x}}\} + EI\{N_{u3_{,x}}\}^T\{N_{u3_{,x}}\} \\ + \kappa AG\{N_{u2_{,x}} - N_{u3_{,x}}\}^T\{N_{u2_{,x}} - N_{u3_{,x}}\}] \mathrm{d}x \end{aligned} \tag{8}$$

where the subscript x indicates partial differentiation with respect to x, whereas a superscript e denotes elemental quantities. The kinetic energy of the bimorph is expressed as (Petyt, 1990):

$$T = \frac{1}{2}\int_0^L \rho A\left(\dot{u}^2 + \dot{v}^2\right) \mathrm{d}x + \frac{1}{2}\int_0^L \rho I\dot{\theta}^2 \mathrm{d}x \tag{9}$$

which can also be expressed as:

$$T = \frac{1}{2}\left\{\dot{\delta}_u^e\right\}^T [M_{uu}^e]\left\{\dot{\delta}_u^e\right\} \tag{10}$$

where

$$[M^e_{uu}] = \frac{1}{2}\int_0^L \rho A\left[\{N_{u1}\}^T\{N_{u1}\} + \{N_{u2}\}^T\{N_{u2}\}\right] + \rho I\left[\{N_{u3}\}^T\{N_{u3}\}\right]\mathrm{d}x \quad (11)$$

The electrical potential energy is given by:

$$U_{\text{elec}} = \frac{1}{2}\int \{D\}^T\{E_3\}\mathrm{d}V = \frac{1}{2[\varepsilon]}\int\left[\{D\}^T\{D\} - \{D\}^T[e]\{S_3\}\right]\mathrm{d}V \quad (12)$$

Imposing the shape functions as defined in Equation (5) and expressing the strain energies of the upper and lower piezoelectric layers gives:

$$U^e_{\text{elec}} = \frac{1}{2}\{\delta^e_d\}^T[K_{dd}]\{\delta^e_d\} - \{\delta^e_d\}^T[K_{ud}]\{\delta^e_u\} \quad (13)$$

where:

$$[K^e_{dd}] = \int_0^L\left[\frac{bh}{2[\varepsilon]}\left(\{N_{d1}\}^T\{N_{d1}\} + \{N_{d2}\}^T\{N_{d2}\}\right)\right]\mathrm{d}x \quad (14)$$

and

$$[K^e_{ud}] = \frac{1}{2}\int_0^L\left[\frac{bh}{2[\varepsilon]}\left(\{N_{d1}\}^T\{N_{u1_{,x}}\} + \{N_{d2}\}^T\{N_{u1_{,x}}\}\right)\right]\mathrm{d}x - \frac{1}{2}\int_0^L\left[\frac{b[e]h}{8[\varepsilon]}\left(\{N_{d1}\}^T\{N_{u3_{,x}}\} + \{N_{d2}\}^T\{N_{u3_{,x}}\}\right)\right]\mathrm{d}x \quad (15)$$

The non-conservative piezoelectric forces are given by:

$$Q_d = \int_0^L V^U\{N_{d1}\}b\mathrm{d}x + \int_0^L V^L\{N_{d2}\}b\mathrm{d}x \quad (16)$$

The element equations of motion are then obtained by using Lagrange's equation. Upon assembly, the equations of motion for the coupled electro-mechanical system are given by:

$$\begin{bmatrix}[M_{uu}] & 0\\ 0 & 0\end{bmatrix}\begin{Bmatrix}\ddot{\delta}_u\\ \ddot{\delta}_d\end{Bmatrix} + \begin{bmatrix}[K_{uu}] & -[K_{ud}]^T\\ -[K_{ud}] & [K_{dd}]\end{bmatrix}\begin{Bmatrix}\delta_u\\ \delta_d\end{Bmatrix} = \begin{Bmatrix}Q_u\\ Q_d\end{Bmatrix} \quad (17)$$

By using the second set of equations of (17), the equations of motion can be reduced to:

$$[M_{uu}]\{\ddot{\delta}_u\} + \left[[K_{uu}] - [K_{ud}]^T[K_{dd}]^{-1}[K_{ud}]\right]\{\delta_u\} = \{Q_u\} + [K_{ud}]^T[K_{dd}]^{-1}\{Q_d\} \quad (18)$$

which can be solved for the structural domain.

The electrical degrees of freedom can be recovered through:

$$\{\delta_d\} = [K_{dd}]^{-1}\{Q_d\} + [K_{dd}]^{-1}[K_{ud}]\{\delta_u\} \quad (19)$$

In this way, the bimorph response can be obtained for any prescribed structural and/or electrical loads. This model will be used to study the dynamics of a linear piezomotor, as described in the following section.

NUMERICAL AND EXPERIMENTAL RESULTS

The results obtained by the numerical simulation and experimental validation of the piezomotor behavior under various loading conditions are presented in this Section. The dimensions and effective material properties of the piezoelectric elements are listed in Table 1.

While the overall dimensions of the piezoelectric bimorphs can be measured, only the active elements contribute to the motion mechanism, as pointed out by Simu and Johansson (2006). In the present design, insulating layers are provided at the sidewalls of the bimorphs to avoid short-circuiting, and also between the electrodes of each piezoelectric layer.

Free Bimorph

To begin with, the drive rod was removed and the piezoelectric bimorphs were allowed to vibrate freely under the action of the imposed voltage excitation. The transverse tip displacement was monitored using a scanning laser Doppler vibrometer. The fundamental natural frequency of each bimorph was calculated to be around 77 kHz. Figure 3 shows the experimentally measured input voltage to the piezoelectric bimorphs during forward backward movements of the drive rod. Inspection of the plots reveals that the supply voltage varies in an almost trapezoidal manner with an amplitude of 24 V and frequency of 925 Hz, which is well beneath resonance allowing room for further increase in operating frequency. Every bimorph is driven by a pair of excitations that are phase shifted by 90°. Of the four bimorphs forming the piezomotor, two are driven in-phase with one another, whereas the other two are driven out-of-phase. The slight deviation from the

Table 1. Bimorph dimensions and piezoelectric properties.

Length, L	3.5 mm
Width, w	3 mm
Thickness, h	1.35 mm
Piezoelectric strain constant, d_{33}	4.76×10^{-8} m/V
Elastic modulus, E	63 GPa
Density, ρ	7600 kg/m^3
Permittivity at constant stress, ε	5×10^{-5} F/m
Shear modulus, G	20 GPa

perfect trapezoidal waveforms is due to the circuitry used to generate these signals.

To simulate the above behavior analytically, only one bimorph is considered and subjected to the trapezoidal voltage signal shown in Figure 4. A small artificial proportional damping term, in the form $[C] = 2\times\ 10^{-5}\ [K]$, has been added in the theoretical model to account for the damping provided by the packing and insulating layers.

The equations of motion are integrated numerically using the Newmark scheme to yield the time response which is used to plot the trajectory of the bimorph tip shown in Figure 5. The trace of the bimorph tip motion resembles a rhombus, in agreement with (PiezoLEGS) and indicates a maximum transverse displacement of $\sim$1.24 μm. Accordingly, the velocity of an unloaded piezomotor is $\sim$4.59 mm/s. Figure 6 shows a comparison of the tip velocity, as measured experimentally, with that obtained theoretically which are in fair agreement. The slight variations observed experimentally can be attributed to errors in supplying truly trapezoidal voltage waveforms.

Loaded Bimorph

The external mechanical loads imposed by the drive rod on the bimorphs during operation consist of both axial loading and transverse friction forces, as suggested by the free-body diagram in Figure 7. Contact between the drive rod and bimorphs is maintained by a preload provided by a spring pushing on a pair of rollers, as indicated. It is assumed that the rollers exert only a normal force N on the drive rod. At the instant shown, two bimorphs are driving the rod to the right through an available friction force $N/2$, being the coefficient of friction. A load, L_o, is also applied externally on the drive rod, as shown.

The axial and shear forces, in N, on each bimorph are assumed to vary periodically in the manner depicted in Figure 8. The abrupt changes in axial and shear forces may be reduced in practice by the drive sequence to ensure smoother load transfer and sharing among the bimorphs.

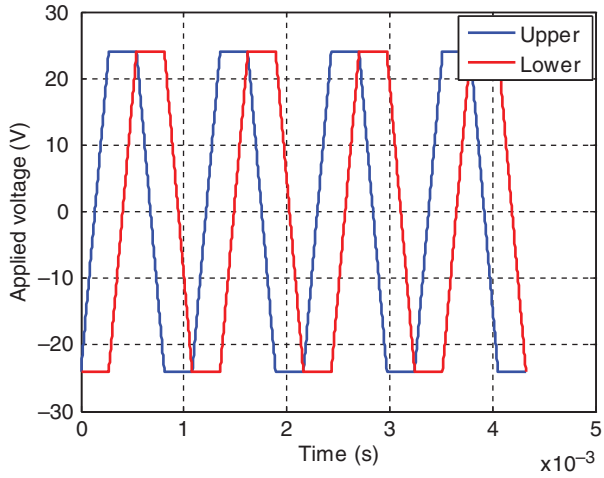

Figure 4. *Trapezoidal voltage input signal to the bimorph.*

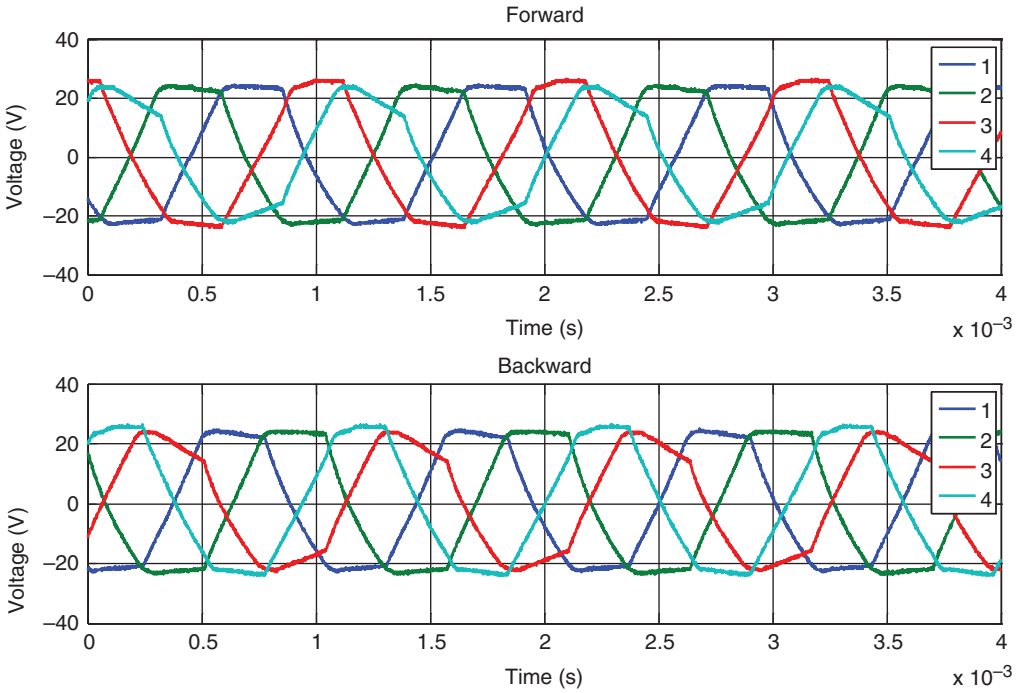

Figure 3. *Experimentally measured input voltage to the piezoelectric bimorphs during forward backward movements of the drive rod.*

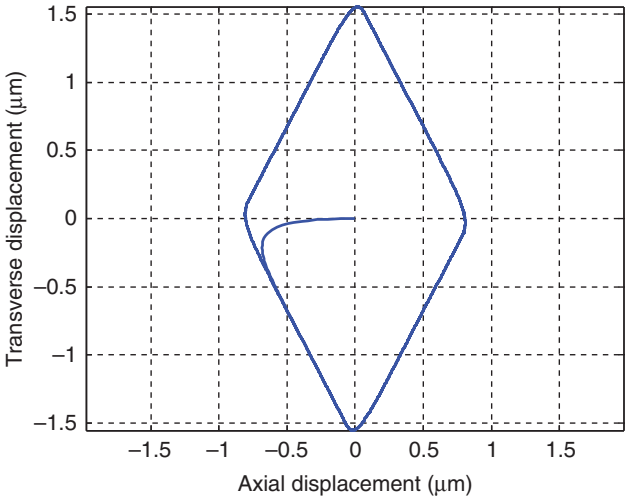

Figure 5. *Trajectory of the bimorph tip.*

The resulting tip trajectory for an axial load of 25 N and shear load 2.5 N is shown in Figure 9.

The piezomotor is then tested experimentally under various external loads by hanging known dead weights attached to the drive rod via a string and measuring the displacement of the drive rod with a laser sensor as shown in Figure 10.

The experimental velocity–load relationship is shown in Figure 11 for both upward and downward motions of the piezomotor. These variations can fairly be approximated by straight line, as indicated.

Based on experimental observations, the velocity of the drive rod was found to decrease with increasing load when lifting the load. The opposite occurred during load lowering. As in friction-driven motors, when the drive rod was stalled, the piezoelectric bimorphs still moved in sliding friction with the drive

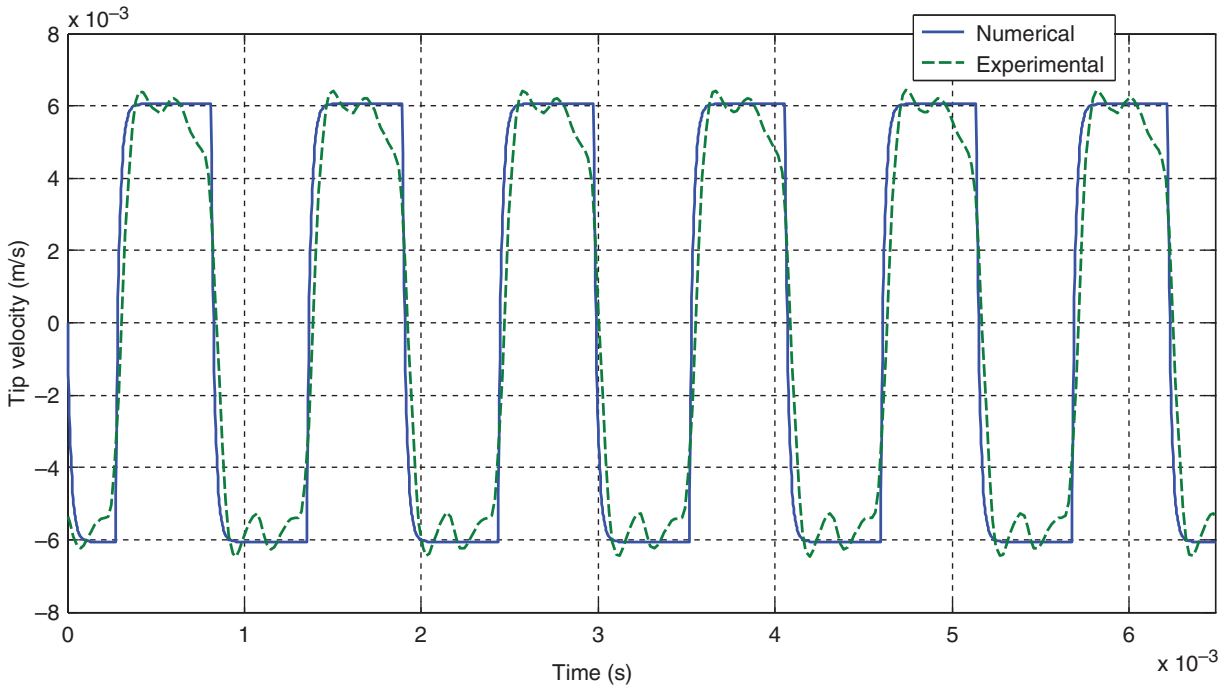

Figure 6. *Comparison between the theoretical and experimental tip velocity.*

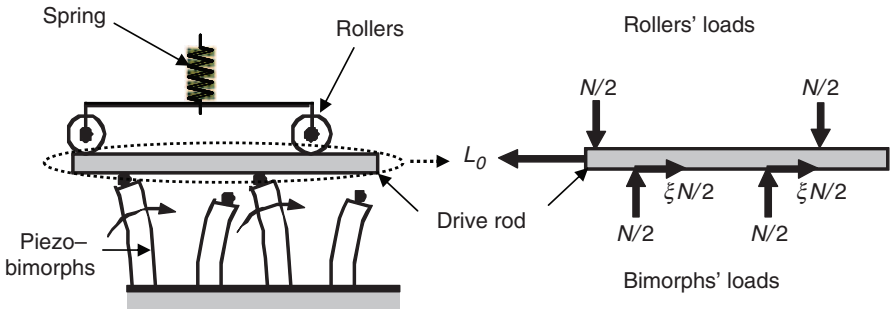

Figure 7. *Schematic model of piezomotor and free body diagram of drive rod.*

rod, but providing insufficient friction force to move the block load. At zero load, a state of 'stick' exists, during which the velocity of the bimorph tips is completely transferred to the drive rod. As the applied external load increases, slipping commences and the drive rod velocity drops. Accordingly, the drive rod velocity, v, can be expressed as:

$$v = V - v_s \tag{20}$$

where V is the velocity of the bimorph tip, and the relation accounts for the loss in drive rod velocity due to slippage. It was also observed that constant steady-state velocities were achieved for various loads. At constant velocity, the driving friction force is given by:

$$f = \mu N = L_0 \tag{21}$$

A Coulomb friction model offers a constant coefficient of friction (hence a constant traction force), regardless of the slip velocity, and hence cannot be used in the present model to capture the experimental observations. As a remedy to this problem, other models have been proposed in the literature (Olsson et al., 1998).

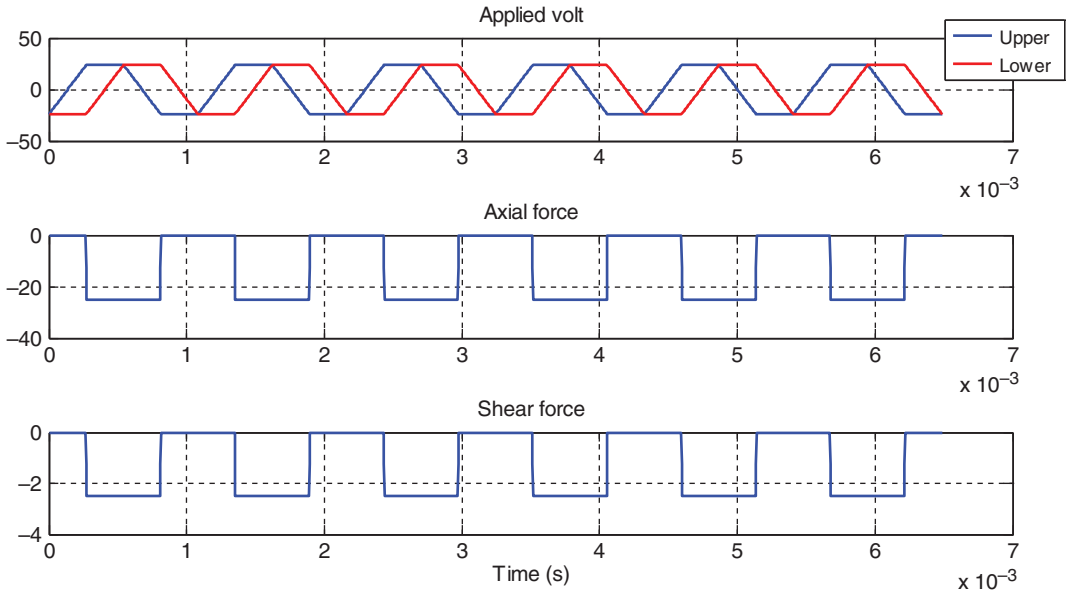

Figure 8. *Periodic variation of the axial and shear forces on each bimorph.*

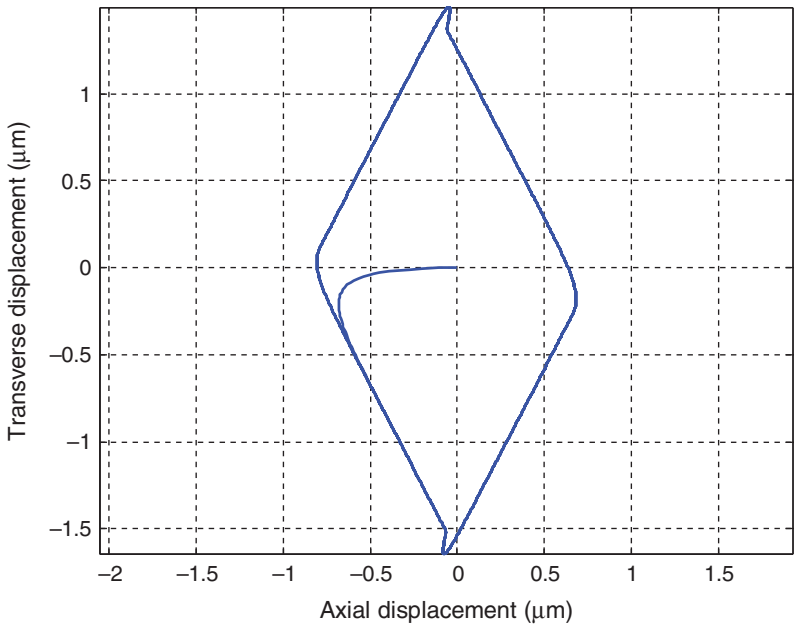

Figure 9. *Tip trajectory for an axial load of 25 N and shear load of 2.5 N.*

Based on the current experiments, we can approximate the velocity–load characteristics during lifting as:

$$v = 5.072 - 0.64L_0 \tag{22}$$

and for lowering as:

$$v = 5.223 - 0.49L_0 \tag{23}$$

where v is in mm/s and L_0 is in Newtons. Comparing Equation (20) with (22) and (23) reveals that according to PiezoLEGS, the normal (axial) force exerted on the bimorphs is around 50 N. Hence, the coefficient of friction relates to the slip velocity through $\mu = 0.0625v_s$ during lifting $\mu = 0.081v_s$ during lowering.

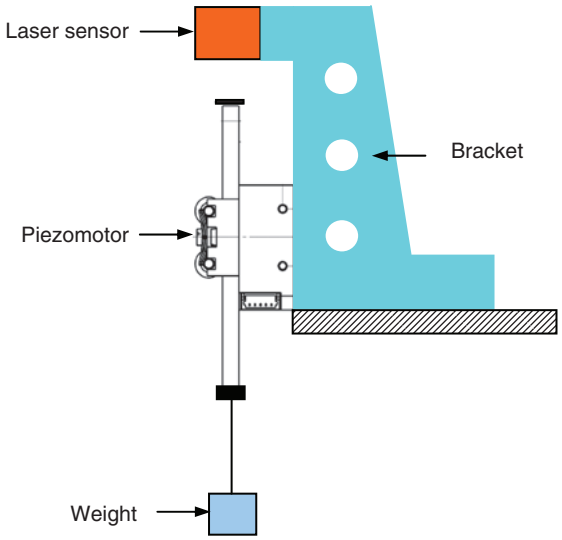

Figure 10. *Experimental set-up for testing the piezomotor.*

CONCLUSIONS

This paper has presented a modeling of the dynamics of a linear piezomotor of the walking type. The developed model is used to predict the piezomotor response to various loads and excitation schemes. It is important here to note that developed model of the piezo-motor presents a comprehensive modeling of this class of motors based on detailed coupled-field finite element model. This is unlike the available models which are based on either quasi-static analysis of the motor dynamics (Simu and Johansson, 2006), or simple second order models which are obtained through system identification for control purposed (Merry *et al.*, 2009).

Furthermore, the developed model simulates the interaction between the dynamics of the piezoelectric bimorphs and the drive rod. An appropriate friction model is used to account for the friction between the bimorph and the drive rod, which is critical to the effective operation of the motor. Experimental testing of the motor is carried out to validate the predictions of the theoretical model.

It is important to note that the piezoelectric bimorph motors have been considered for this study because of their high output power, lower applied electric field, high stiffness, and accurate load positioning capabilities. However, these performance metrics occur at the expense of higher motor weight, low travel speeds, and low overall efficiency.

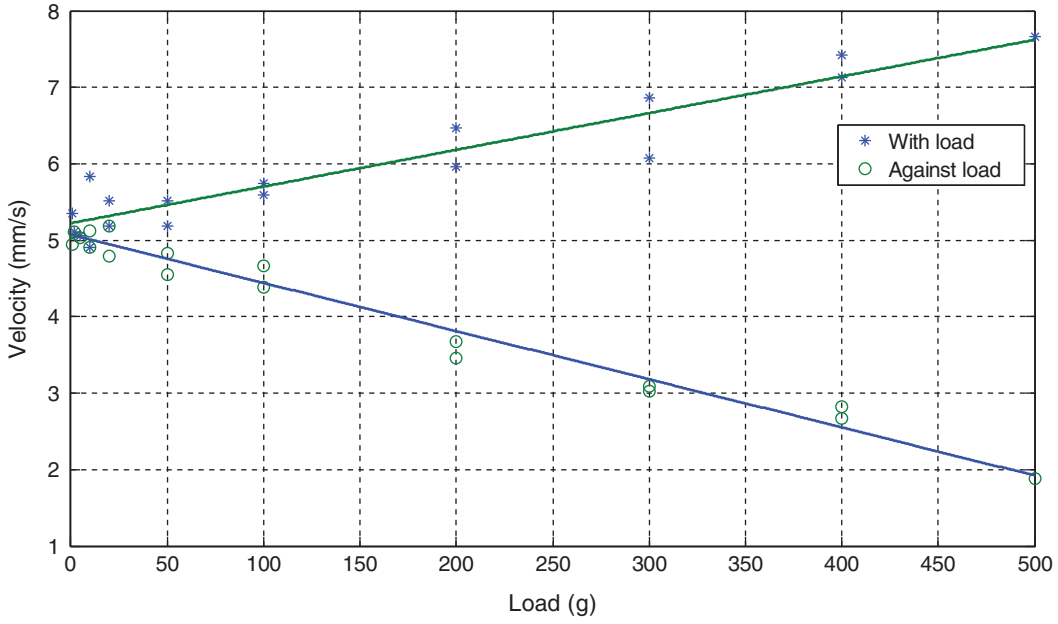

Figure 11. *Velocity of piezomotor as function of applied load.*

This effort aims ultimately at demonstrating the feasibility of employing this class of piezoelectric actuators in driving various smart systems.

ACKNOWLEDGMENTS

We wish to thank Dr Mats Bexell of PiezoMotor AB for providing the piezoelectric properties of the bimorphs. This work has been funded by King Abdulaziz City for Science and Technology (KACST) Grant # 28-115. Special thanks to Prince Dr Turki bin Saud bin Mohammed Al Saud, KACST VP, the technical monitor, for his invaluable technical inputs and support.

REFERENCES

Bexell, M. and Johansson, S. 1999. "Fabrication and Evaluation of a Piezoelectric Miniature Motor," *Sensors and Actuators*, 75:8–16.

Chang, W.S. and Youcef-Toumi, K. 1998. "Modeling of an Omni-Directional High Precision Friction Drive Positioning Stage," In: *Proceedings of the 1998 IEEE International Conference on Robotics and Automation*, Leuven, Belgium, pp. 175–180.

Friend, J., Umeshima, A., Ishii, T., Nakamura, K. and Ueha, S. 2004. "A Piezoelectric Linear Actuator Formed from a Multitude of Bimorphs," *Sensors and Actuators A: Physical*, 109:242–251.

Hill, C. 2002. Piezoelectric Motor, U.S. Patent No. 6,373,170B1.

Johansson, S., Bexell, M. and Litchell, P.O. 2002. Fine Walking Actuator, U.S. Patent No. 6,337,532.

Johansson, S., Bexell, M. and Jansson, A. 2004. Fine Control of Electromechanical Motors, US Patent No. 2004/0007944A1.

Johansson, S., Abrahamsson J. and Sunnerberg R. 2008. Wide Frequency Range Electromechanical Actuator, US Patent No. 7,355,325.

Merry, R.J.E., de Kleijn, N.C.T., van de Molengraft, M.J.G. and Steinbuch, M. 2009. "Using a Walking Piezo Actuator to Drive and Control a High-Precision Stage," *IEEE/ASME Transactions on Mechatronics*, 14:21–31.

Olsson, H., Aström, K.J., Canudas de Wit, C., Gäfvert, M. and Lischinsky, P. 1998. "Friction Models and Friction Compensation," *European Journal of Control*, 4:176–195.

Piezo LEGS. 2009. Data and User Instructions, PiezoMotor Uppsala AB, Sylveniusgatan 5D, Sweden Available at: http://www.piezomotor.se/

Petyt, M. 1990. *Introduction to Finite Element Vibration Analysis*, Cambridge University Press, Cambridge, MA.

Simu, U. and Johansson, S. 2006. "Analysis of Quasi-Static and Dynamic Motion Mechanisms for Piezoelectric Miniature Robots," *Sensors and Actuators A: Physical*, 132:632–642.

Simu, U. and Johansson, S. 2002. "Fabrication of Monolithic Piezoelectric Drive Units For A Miniature Robot," *Journal of Micromechanics and Microengineering*, 12:582–589.

Smits, J.G., Dalke, S.I. and Cooney, T.K. 1991. "The Constituent Equations Of Piezoelectric Bimorphs," *Sensors and Actuators A*, 28:41–61.

Tani, K., 1996. "Friction Models for a Mobile Machine Using Piezo Vibration", In: *Proceedings of the fourth International Workshop on Advanced Motion Control (AMC, 96)*, Vol. 2, Tsu-city, Mie-Hen, Japan, March 18–21, pp. 717–722.

Tieck, R.M., Emmons, M.C. and Carman, G.P. 2007. "Alternate Evaluation Criteria of Piezoelectric Motors," *Journal of Intelligent Material Systems and Structures*, 18:1215–1221.

Vinhais H.F., Ibrahim R.C. and Silva E.C.N., 2004. "Simulation of a Linear Piezoelectric Motor by Using Finite Element Method," In: *ABCM Symposium Series on Mechatronics*, Adamowski, J.C., Tamai, E.H., Villani, E. and Miyagi, P.E. (eds), Vol. 1, Rio de Janeiro, Brazil, pp. 697–706.

Wang, S.Y. 2004. "A Finite Element Model for the Static and Dynamic Analysis of a Piezoelectric Bimorph," *International Journal of Solids and Structures*, 41:4075–4096.

Youn, S-.K. and Becker, E.B. 1991. "A Coupled Field Beam Theory for Piezoelectric Biomorphs," *Ferroelectrics*, 119:41–52.